INTERFACIAL CRACK VELOCITIES IN A SNOW SLAB – NUMERICAL SIMULATION

P. Mahajan* and S. K. Joshi

Department of Applied Mechanics
Indian Institute of Technology Delhi, Hauz Khas, New Delhi - 110016, India

ABSTRACT: A snow pack consists of weak layers embedded in strong layers. The interface bond between a weak layer and layers in between which it is sandwiched may not be strong and there may be regions that are not bonded. The un-bonded regions act as stress raisers from where propagation of crack can take place, in mode II, along the weak interface. The crack propagation along the interface under a shear and compressive load (due to the weight of skier) is studied using cohesive zone elements to describe the interface between the weak and strong layers. Four properties of the interface namely fracture energy in normal separation, fracture energy in shear separation, tensile and shear strengths are needed to characterize the cohesive elements. Tension and shear experiments on sieved snow with an 'ice lens' and shear experiments on field snow with a weak interface are performed to get an estimate of the cohesive zone properties. The cohesive model, incorporated in a finite element mesh, is used to determine the speed of crack growth along the interface. The average cracks speed depends on modulus of the layers on either side of interface and for the modulus values studied here, is between 40 m/s and 200 m/s.

KEYWORDS: cohesive zone, dynamic crack growth, weak layer, snow, finite element

1. INTRODUCTION

A snow pack on the slope is rarely homogenous and consists of a number of layers of varying microstructure, properties and strength. Cracks in the weak layers embedded in the layered snow pack act as stress raisers which reduce the strength of the whole snow pack. The cracks may be formed, as the sandwiched weak layers may not adhere to the strong layers in some regions. In remaining regions a bond between the layers may be formed but its strength is much lower than the strength of layers themselves. Under sustained shear loads due to gravity load or overloads due to skier or fresh snowfall this weak bond strength may be easily exceeded and propagation of crack along the interface causes slab failure and an avalanche to occur. Interfacial failure as a mechanism of avalanche initiation is well recognized in literature. McClung (1987) has stated "first failure will occur in or at boundaries of the weak layer".

* *Corresponding author address:* Puneet Mahajan, Department of Applied Mechanics, Indian Institute of Technology, Hauz Khas, New Delhi-16; tel: 91-11-26591229; fax: 91-11-26581119; email: mahapun@hotmail.com

Similarly, Schweizer (2002) has observed "the snow pack weakness is either a thin layer or a weak interface where two layers are poorly bonded due to at-least one of the two layers having weak layer properties". He further attributes the grain size difference across the "fracture interface" to be responsible for the poor bonding between the two layers and the hardness difference between the layers "to favor stress/strain concentrations at the interface and promote fracture propagation".

In an earlier paper (Mahajan and Senthil, 2005) (MS) the authors modeled the pack as being made of two strong and one weak layer with cohesive zone elements at the interface between the layers to study interfacial fracture in snow on a slope under its self weight. This involved characterizing material on either side of bond line by suitable constitutive relations and using a cohesive surface constitutive relation for the bond itself. The cohesive surface constitutive law specified the relation between traction and displacement jump across the bond line and allowed for creation of new free surface. These relations were incorporated in a finite element (FE) mesh to study crack initiation and propagation. One of the major advantages of the technique is its ability to initiate a crack in the absence of an initial crack. In snow however, it was shown that an initial crack of a certain size is essential before the crack will grow. As

explained by MS the use of cohesive elements requires a very fine mesh with the smallest elements about 4-5 times the characteristic length (10^{-5} m). This restricted our study to a small slab of snow of length 2 m. Although the crown crack perpendicular to the slope did not initiate in the 2 m of slab it was however seen that the normal stress parallel to the slope increased with crack length. Rahulkumar et al. (2000) have used CZM to describe polymer interfacial fracture during a compressive shear test. They analyzed the transition from stable to unstable fracture and also investigated dynamic crack growth followed by crack arrest and stable crack growth, is investigated. Needleeman and Rosakis (1999) analyzed numerically crack growth along steel- PMMA interface under impact shear loading, using cohesive surface constitutive laws for the interface. For a sufficiently low impact velocity, the crack speed increased smoothly to the PMMA Rayleigh wave speed, whereas above a sharply defined transition impact velocity, the crack speed reached a value somewhat less than the PMMA dilational wave speed.

It is often reported that very rapid avalanche initiation takes place sometimes when a skier accidentally steps on fragile layered snow. In such a situation the crack speeds are likely to be high causing very rapid crack growth and subsequent avalanche initiation. Crack velocities of the order of 10^2 - 10^3m/s have been predicted by Bader and Salm (1990) for a brittle crack in snow. Fracture propagation speed of 20 m/s, through a weak layer in snow on low angled terrains, were measured using geophones by Johnson et al.(2004).The authors explained this speed as the speed of flexural wave. McClung (2005) offered an alternative view, namely that propagation speeds were due to crack propagations speed of mode II and mode III fracture. He predicted the shear rupture speeds in the range 0.7–0.9 $Cs = 0.7\text{-}0.9(G/\rho)$ which for shear modulus G = 0.3 MPa yielded shear rupture speeds in the range 28–36 (m/s) close to the ones measured by Johnson et al. The shear modulus is however an order of magnitude lower than the one used by Wilson et al. (1999) in their FE studies. Wilson et al. have performed plane strain static (FE) analysis to study on how warming in the top 20 cm of a hard 'spring' like snowpack and a softer 'mid-winter' like snowpack influence the stresses and strains due to a skier load in weak layers 30 and 50 cm below the surface. The snow stiffness varied between 10 MPa for very hard snow to 0.25 MPa for very soft snow. A point load of 500N/m was applied to the model and it was the components of this load which were acting on the 6 m long snow pack. Recently, Herwijnen and Jamieson (2005) observed crushing of the weak layer due to fracture in the weak layer and from the displacement of the markers placed in the snow layer above the weak layers determined the crack velocity in snow in the range of 17-26 m/s.

Few numerical estimates for these crack velocities exist and here we use FE and CZM to study rapid crack growth and estimate the crack velocity in a snow slab under compressive and shear loads similar to the load conditions present during skiing. The weak layer is assumed to remain intact and crack propagation is due to rupturing of the bonds between the strong and weak layer. Since we are interested in crack speeds a dynamic analysis is performed. The load is suddenly applied at time t = 0 and even though it remains constant thereafter, the stresses within the pack change due to wave propagation and change in crack length. The load component along the slope in study of Wilson et al. was component of weight along the slope. Here, the component of force along the slope arises from friction between the ski and the snow.

The properties of the cohesive zone elements, used at the interface between the strong and weak layer, are estimated for two different types of interfaces by performing separate tension and shear experiments. In laboratory experiments the interface was an 'ice lens' with sieved equi-temperature ET snow on either side. In the field snow the interface occurred at the boundary between decomposed and highly faceted grains.

2. CONSTITUTIVE LAWS FOR SNOW LAYERS AND COHESIVE ELEMENTS

Snow is a granular material with ice as matrix material and its constitutive behavior is a function of its microstructure (Mahajan and Brown, 1992). Constitutive law of Biot for porous aggregates has been used to study wave propagation in snow by Johnson (1990) and Albert (1993) and can be used to study dynamic crack propagation in avalanches. In most existing crack propagation models for avalanche initiation (e.g. Bader and Salm) the

porous snow is replaced by an equivalent elastic solid. While, in future, it may be more appropriate to include effects of porosity, here we presume snow layers as elastic solid.

2.1 Principle of Virtual work and cohesive elements

To determine the state of stress in the slab shown in figure 1, due to sudden application of constant uniformly distributed pressure and friction loads the principal of virtual work for dynamics is

$$\int_V s:\delta F dv - \int_{S_{int}} T.\delta\Delta dS = \int_{S_{ext}} T.\delta u dS - \int_V \rho \frac{\partial^2 u}{\partial t^2}.\delta u\, dv \quad (1)$$

Here s is the nominal stress tensor and is related to Cauchy stress by the relation $s = F^{-1}$ det Fσ, σ being the Cauchy stress. *F* is deformation gradient, V the volume in the reference configuration, Δ is the virtual jump displacement across the cohesive element faces. V, S_{ext}, S_{int} are the volume, external surface area and internal cohesive surface area of the body in the reference configuration. The density of the material is ρ and T is the traction vector.

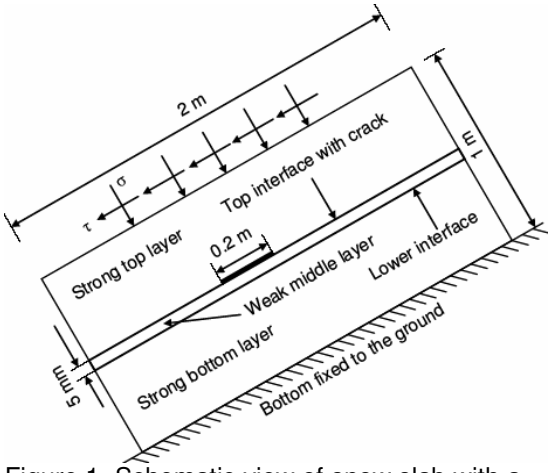

Figure 1. Schematic view of snow slab with a top interfacial crack used in FE simulation. 'σ' is the component of load due to weight of skier, 'τ' is the friction force.

The various layers in slab are assumed to be isotropic elastic with two elastic constants E and υ the Modulus of Elasticity and Poisson's ratio respectively. There can be a wide variation in properties of snow depending on its density and hardness [Mellor(1975)]. As equation 2 below shows the wave velocities (and therefore the crack propagation velocities) in elastic medium depend on its elastic modulus and density. The dilatational, shear and Rayleigh wave velocities in the strong and weak layer are calculated using

$$C_L = \left\{ \frac{E}{\rho}\left[\frac{(1-\upsilon)}{(1+\upsilon)(1-2\upsilon)} \right] \right\}^{1/2},$$

$$C_T = \sqrt{\frac{G}{\rho}},$$

$$C_R = \frac{0.862 + 1.14\upsilon}{1+\upsilon} C_T \quad (2)$$

For snow, approximated as a non-porous continuum, these velocities will vary depending on the type of snow. Simulations are done for three different values of the modulus of the strong (E_s) and weak (E_w) layers. These are (i) E_s = 10 MPa, and E_w = 1 MPa (ii) E_s = 1 MPa and E_w as 0.1 MPa. (iii) E_s = 1 MPa and E_w = 0.75 MPa. For all cases the density ρ of strong layer is 300 kg/m^3 and that of weak layer is 100 kg/m^3. The various wave velocities corresponding to these moduli are given in table 1.

Table 1. Wave velocities in snow

E (MPa)	ρ (Kg/m^3)	C_L	C_T	C_R
10^7	300	196.57	116.41	106.39
10^6	300	62.16	36.81	33.64
	100	107.67	63.76	58.27
7x10^5	100	90.08	53.34	48.76
10^5	100	34.05	20.16	18.43

Next, the constitutive law for zero thickness cohesive surface elements that are introduced between boundaries of elements, at the interface, in a normal finite element mesh is briefly presented. The cohesive elements, as considered by Xu and Needleman (1994), are characterized by a stress-opening displacement potential function ϕ which allows for both tangential as well as normal separation.

$$\phi(\Delta) = \phi_n + \phi_n \exp\left(-\frac{\Delta_n}{\delta_n}\right) \left\{ \left[1 + \frac{\Delta_n}{\delta_n} \right] \left\{ q\left[1 - \exp\left(-\frac{\Delta_t^2}{\delta_t^2} \right) \right] - 1 \right\} \right\} \quad 3)$$

Here ϕ_n is the work of normal separation, q = ϕ_n / ϕ_t and ϕ_t is the work of tangential separation. In the above expression the

subscripts *n* and *t* indicate the normal and tangent components respectively. Here **n** and **t** are normal and tangent respectively to the surface a given point in the reference configuration, then $\Delta_n = \mathbf{n}.\boldsymbol{\Delta}$ and $\Delta_t = \mathbf{t}.\boldsymbol{\Delta}$.

The tractions **T** and displacement jump vectors **Δ** across the surface are related by

$$T = \frac{\partial \phi}{\partial \Delta} \tag{4}$$

As the cohesive surfaces separate, the magnitude of the traction at first increases to a maximum and then approaches zero with increase in separation. Xu and Needleman considered the constitutive relation for each cohesive surface as elastic, so the dissipation associated with separation is neglected. From equations (3) and (4) the cohesive surface tractions are written as

$$T_n = \frac{\phi_n}{\delta_n} exp\left(-\frac{\Delta_n}{\delta_n}\right)\left\{\frac{\Delta_n}{\delta_n} exp\left(-\frac{\Delta_t^2}{\delta_t^2}\right) + (1-q)\left[1-exp\left(-\frac{\Delta_t^2}{\delta_t^2}\right)\right]\frac{\Delta_n}{\delta_n}\right\}$$

$$T_t = -\frac{\phi_n}{\delta_n}\left(2\frac{\delta_n}{\delta_t}\right)\frac{\Delta_t}{\delta_t}\left\{q\left(1+\frac{\Delta_n}{\delta_n}\right)\right\} exp\left(-\frac{\Delta_n}{\delta_n}\right) exp\left(-\frac{\Delta_t^2}{\delta_t^2}\right) \tag{5}$$

The normal work of separation, ϕ_n, and the shear work of separation, ϕ_t can be written as

$$\phi_n = e\,\sigma_{max}\,\delta_n \;;$$

$$\phi_t = \sqrt{\left(\frac{e}{2}\right)}\,\tau_{max}\,\delta_t \tag{6}$$

where e = exp(1), σ_{max} and τ_{max} are the cohesive surface normal strength and tangential strength respectively, and δ_n and δ_t are the corresponding interface characteristic lengths.

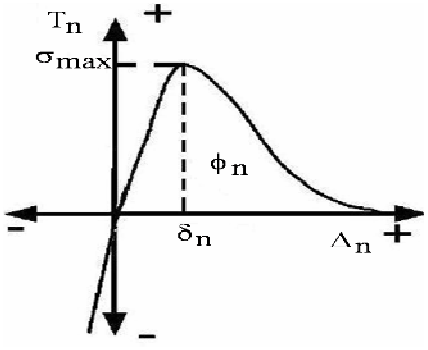

Figure 2. (a) Normal traction, T_n, across the cohesive surface as a function of normal separation δ_n.

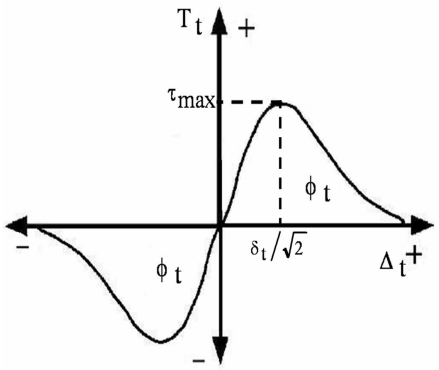

Figure 2. (b) Shear traction, T_t, across the cohesive surface as a function of tangential separation δ_t.

Fig. 2a shows the normal traction T_n across the surface as a function of Δ_n with $\Delta_t \equiv 0$. The maximum value of T_n is σ_{max} and it occurs when $\Delta_n = \delta_n$. Fig. 2b shows the shear traction T_t across the cohesive surface as a function of Δ_t with $\Delta_n \equiv 0$. The maximum value of $|T_t| = \tau_{max}$ is attained when $|\Delta_t| = \delta_t/\sqrt{2}$. The cohesive surface elements are implemented numerically as a User Element in ABAQUS (Hibbit, 2005). A penalty approach is used to prevent interpenetration of layers under compressive loads.

From above, it is clear that CZM can be described by four parameters ϕ_n, ϕ_t, σ_{max} and τ_{max}. In general the cohesive energy ϕ is obtained from experiments and is equivalent to work of fracture. For snow, only limited information exists for these parameters. On basis of the experiments Kirchner et al. (2002) quote a value of 0.125 J/m^2 for work of fracture for low density snow. No experimental data exists for interfacial fracture energy or strength and in our previous paper we used a value of 0.05 J/m^2 for both ϕ_n and ϕ_n, and 0.00184 MPa and 0.004 MPa for normal and shear interface strengths. These values correspond to $\delta_n = \delta_t = 10^{-5}$ m

3. DETERMINATION OF COHESIVE ZONE PARAMETERS – EXPERIMENTS AND FINITE ELEMENT SIMULATIONS

To get a better estimate of the cohesive zone properties tension and shear experiments were performed on sieved snow with an 'ice lens' and in field conditions on snow with an interface between decomposed and highly faceted grains. The experiments on

layered snow were next simulated by finite element method to determine ϕ_n, ϕ_t, δ_n and δ_t as briefly discussed below.

3.1 Sample preparation of laboratory specimens

Tension and simple shear experiments on layered samples were performed both in Cold laboratory and field conditions at -10^{0}C. In the cold laboratory six samples of sieved snow were prepared for this experimental analysis. The samplers were filled with sieved snow (fine grained snow of grain size 0.5 mm to 1.0 mm). Cylindrical samples of 65 mm diameter and 150 mm height were chosen for tension tests. Rectangular samples of 150 mm x 75 mm x 70 mm were chosen for shear tests.

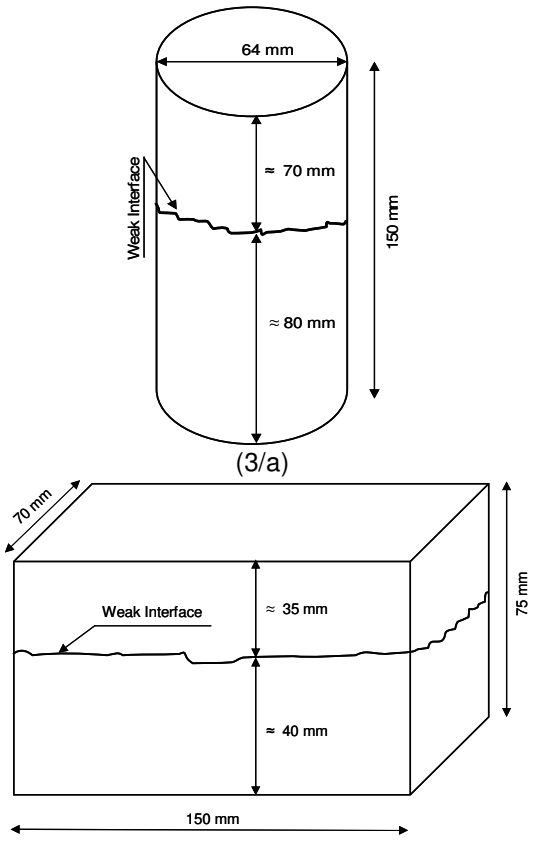

Figure 3. Specimens for a) tension test and b) shear test.

Each sample was initially made in two pieces of heights 80 mm and 70 mm for tension specimens and 40 mm and 35 mm for shear specimens (figure 3a and 3b).

A weak interface was made by putting a heated plate at the top surface of lower piece thus creating a water layer at this surface. This water layer was frozen rapidly and the two pieces were put together and allowed to sinter for seven days. The ice layer or lens introduced in the sample had an approximate thickness of 1.5 mm. The prepared samples were loaded in tension. Figure 4 shows two representative load-deformation curves from tension tests conducted at a constant strain rate of 10^{-4}/s and 10^{-5}/s. Experiments on homogeneous sieved snow, without an interface, were also conducted to determine the modulus of the top and bottom layers.

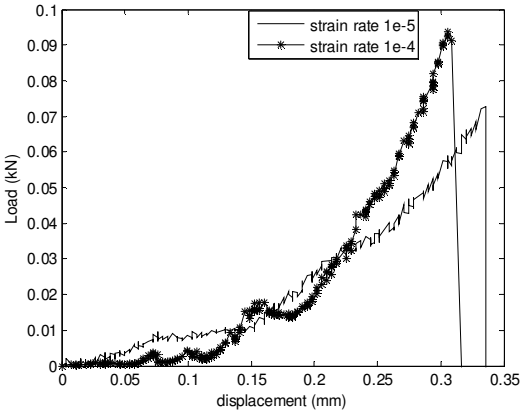

Figure 4. Tension tests on layered snow with an 'ice lens' at two different strain rates.

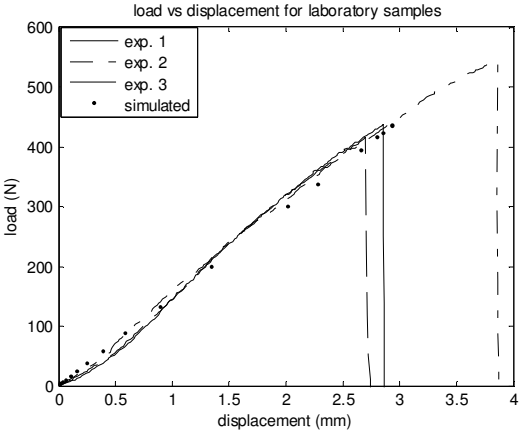

Figure 5. Shear tests on layered snow with an 'ice lens' at a strain rate of 10^{-4}/s. E = 3 MPa, density = 330 kg/m^3.

Figure 5 shows load deformation curves for the sieved snow samples in plane shear for a strain rate of 10^{-4}/s.

In years 2005 and 2006 a range of field samples with different interfaces were also collected from various slopes and tested

under plane shear. Shear tests were done on the various interfaces found within the snowpack by cutting the snow bocks of size 150mm x 75mm x 70mm. The grains on either side of

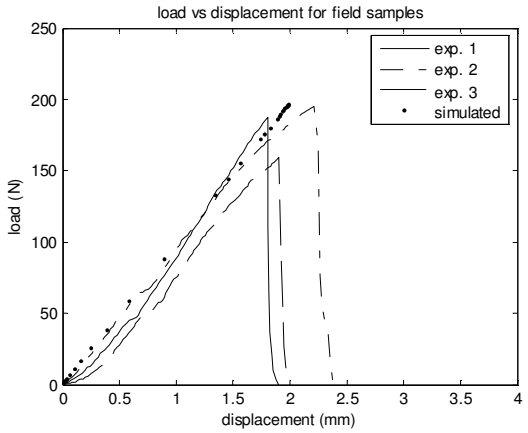

Figure 6. Shear tests on layered field snow with an interface between decomposed and highly faceted grains at a strain rate of 10^{-4}/s.

interface were of different type. The load deformation curve for snow with decomposed snow (felt like) on one side and highly faceted grains on other side of interface at a strain rate of 10^{-4}/s is shown in figure 6. Samples were also tested at 10^{-5}/s although the graphs are not shown here. In the experiments failure occurred at the interface and snow on either side of interface did not fail.

3.2 Static FE simulation to predict cohesive zone properties

The load deformation experiments on layered snow are next simulated using static non-linear plane strain finite element (FE) analysis for shear specimens and axi-symmetric analysis for tension specimens. Different interfaces have different cohesive properties and here estimates are established for tests shown in figures 4 to 6. As mentioned earlier figures 4 and 5 are for laboratory samples with an ice lens whereas figure 6 is for field specimens. E for laboratory snow was taken as 3 MPa based on experiments on homogeneous snow without interface. The weak interface was represented by cohesive elements. For tension tests at strain rate of 10^{-4}/s various values of cohesive zone parameters (ϕ_n and δ_n) were tried so that FE load-displacement curves matches with the experimental curves. An average value for ϕ_n = 0.05 J/m^2 and $\delta_n = 10^{-5}$ m was obtained from this analysis. The slope of the load displacement curve depended on the Young's modulus of snow whereas the displacement at which the load dropped depended on fracture energy and characteristic length values. For laboratory tests using the value of ϕ_n and δ_n determined in tension, a plane strain static FE analysis of shear test was performed. ϕ_t and δ_t were calculated by hit and trial so as to match the experimental and FE prediction of load displacement curve (fig.6). For both tension and shear the FE analysis had to be stopped, due to convergence problems, once the load dropped after reaching a peak and complete load-displacement curve beyond this load could not be traced. For shear tests, performed in the cold laboratory at a strain rate of 10^{-4}/s an average value of ϕ_t was 0.025 J/m^2 and δ_t was 5 x 10^{-6} m.

For tests in the field, it was assumed that the modulus of layers on either side of interface was same and the slope of load displacement, ϕ_t and δ_t were suitably approximated to match the experimental and simulated load-displacement curves. Tension tests were not performed on the field snow. For interface between felt like and faceted crystals, obtained in the field, both simulated and experimental load displacement curves are shown in figure 6. For this interface ϕ_t was 0.015 J/m^2 and δ_t was 8 x 10^{-6} m. Here, in simulations in section 4 for snow slab loading, we have used ϕ_n = 0.05 J/m^2, ϕ_t = 0.01 J/m^2, $\delta_n = \delta_t = 10^{-5}$ m.

4. SNOW SLAB LOADING AND CRACK GROWTH SIMULATIONS

The crack propagation problem in a slab with a moving skier at top involves solving contact problem between the skier and snow and simultaneously using cohesive elements for studying interfacial crack growth under dynamic conditions. This can be very time consuming as the use of cohesive elements requires a very fine mesh with the smallest elements about 5-10 times the characteristic length (10^{-5} m). Here, to reduce the solution time we do only a plane strain analysis (1 m wide) and assume the 2 m long slab as being made of three layers- two strong layers in between which a weak layer is sandwiched. The compressive force on snow is due to

normal component of weight of the skier and shear load due to friction between skies and snow are constant and uniformly distributed over one meter length. Coulomb friction is considered and coefficient of dynamic friction is taken as 0.1. A line load of 500 N/m uniformly distributed over a length of one meter was applied on the top, as shown in figure 1. For a slab on a uniform slope of 30^0 the total normal compressive load on slab is 433 N and shear load is 43.3 N. For dynamic solution a fixed time step of 10^{-5} seconds was used although sometimes times it had to be reduced to 10^{-6} s for the solution to converge. The average solution time on xeon dual processor machine for the above problem is approximately two days.

Two different slab thicknesses are analyzed. In first case the block is 1 m deep with a 5 mm thick weak layer, at 50 cms from bottom. In second case, the block is 15 cm deep and has a weak layer, 5 mm thick, at 4.5 cms from the bottom. The bottom of the slab is assumed fixed to the ground. A weak interface occurs on both the sides of the weak layer and cohesive elements are placed at both the interfaces. With cohesive elements the crack can initiate and subsequently propagate even in the absence of an initial crack. An initial crack of 20 cms is introduced on the top interface at centre of the slab approximately. A convergence study was performed for various sizes of the cohesive elements and on the basis of this study size of these elements is taken as 10^{-4} m, i.e., ten times the cohesive element characteristic length. The convergence study concentrated on stresses and displacements in the cohesive region and we found no change in these with further refinement of element size.

The first step in computing the crack speed is to record the crack location. For snow slab lengths considered here, the compressive loads at the top prevent opening of the interface and therefore the crack speeds are computed using shear separation Δ_t and hence are shear crack speeds. The time at which for a given node along the cohesive surface Δ_t first becomes greater than or equal to $5\Delta_t$ defines shear crack location. The $5\Delta_t$ opening defining the crack location is a bit arbitrary and it can happen during numerical calculations that the relative separation between many nodes may be at $4.99\Delta_t$during a particular time increment and therefore these nodes will not be a part of the crack. In the next increment the relative separation between these nodes will exceed $5\Delta_t$ and the velocity calculated for this increment on basis of crack location during this and previous increment may be very high whereas it may have been low during the last increment. To adjust for these fluctuations in velocity a linear best fit is done using velocity at five nodes.

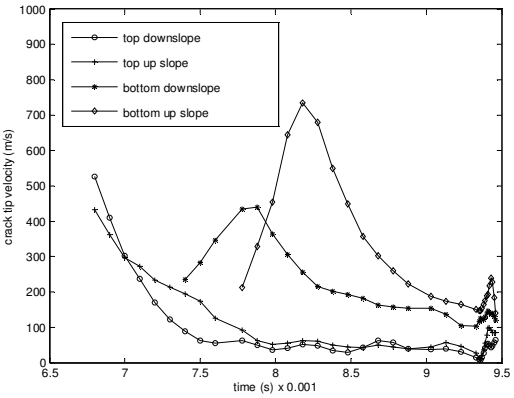

Figure 7. Up-slope and down slope Crack velocity versus time for $E_s = 10^7$ Pa and $E_w = 10^6$ Pa.

The crack velocity versus time graph is shown in figure 7 for $E_s = 10^7$ Pa and $E_w = 10^6$ Pa. The initial crack is there only at the top interface. The crack grows on either side of this initial crack. The initial down-slope crack velocities are high up to 7.5 x 10^{-3} s but subsequently vary between 30 and 100 m/s till 9.5 x 10^{-3} s. At this time the crack velocities dip to 10 m/s before rising again to 95 m/s. A very similar behavior is observed during the up slope crack growth. The final up slope and down slope crack lengths at the top interface are 0.23m and 0.21 m. The average crack velocities are 85m/s and 105 m/s and exceed the C_R and C_s wave velocities of the weak layer but are below the C_L of the weak layer and C_R of the strong layer. At the lower interface, although there is no initial crack, a crack opens by itself at two locations 0.66m and 0.79 m from the left (or the down slope end) and right ends respectively of the slab. The down-slope crack opens at 7.4 x 10^{-3} s and reaches a peak velocity of 470 m/s before slowing down to 200 m/s at the time of fracture. The up slope crack opens later at 7.78 x 10^{-3} s and has a peak velocity of 720 m/s before slowing down to 230 m/s. The average crack velocities at this interface are supersonic exceeding all the wave velocities of the layers on either side of interface. The

lower interface crack velocities are much higher than the upper interface crack velocities and final fracture occurs at the lower interface. A similar simulation run for a thin slab of thickness 15 cms does not show any cracks at the bottom interface and failure occurs due to slipping at the top interface only.

Figure 8 shows the crack velocity versus time graph for $E_s = 10^6$ Pa and $E_w = 10^5$ Pa. The initial down-slope speed is 42 m/s and up slope speed is 65 m/s. Subsequently, both cracks travel at similar speeds close to 40 m/s. At t = 18.7 the crack velocities start reaching 3-4 m/s at 18.9 x 10^{-3} s. At the bottom interface shear separation starts but is small in magnitude. The simulation could not be completed as for the solution to converge, time steps below 10^{-6} seconds were required.

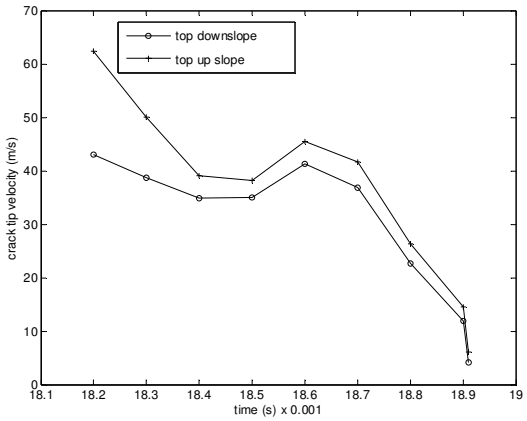

Figure 8. Up-slope and down slope Crack velocity versus time for $E_s = 10^6$ Pa and $E_w = 10^5$ Pa.

Instead of having a middle layer with uniform properties, as tried above, the 5 mm thick middle layer was subdivided into three regions. The top and bottom 1.5 mm were modeled as solid continuum with E = 10^6 Pa. The middle 2.0 mm was modeled as alternating columns of snow and air, each 1.2 mm wide. The effective modulus of the middle layer using the rule of mixtures is approximately 7 x 10^5 Pa. The strong layer modulus is $E_s = 10^6$ Pa. The average down-slope and up slope crack velocities at the top interface are 53 m/s and 40 m/s. The down slope velocity exceeds the C_R of the weak layer but the up-slope velocity is below it. The down-slope and up-slope crack lengths are 0.42 m and 0.43 m respectively. As seen in figure 9 the cracks open at the lower interface in down-slope direction at 21.5 ms and 22.5 ms in the up slope direction. The average velocities on this interface are 83 m/s and 200 m/s. The latter exceeds all wave velocities of the layers on either side of interface.. The final crack lengths on this interface at time of fracture are 0.178 m down-slope and 0.218 m up-slope. The crack speeds at both the interfaces in figure 9 are much slower as compared to values in figure 7. Also, while in figure 7 the lower interface cracks opened quite early, in figure 9 they open quite late in comparison to upper interface cracks.

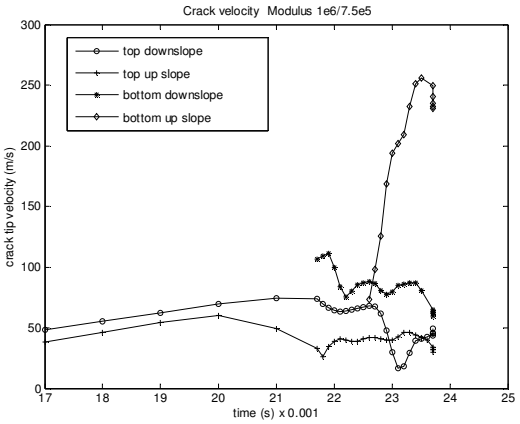

Figure 9. Up-slope and down slope Crack velocity versus time for $E_s = 10^7$ Pa and $E_w = 7$ x10^5 Pa.

CONCLUSIONS

Cohesive zone model is used to study the interfacial fracture in layered snow and determine the crack velocities. Comparison of load-displacement curves from experiments on layered snow, with those from simulations provide an estimate of the cohesive properties. The shear and tension fracture energies are approximately 0.01 J/m^2 and 0.05 J/m^2 and characteristic lengths obtained are about 10^{-2} mm. The crack velocities depend on the modulus of the layers and the behavior of crack depends on the thickness of the slab. In a slab of 1 m thickness the crack growth started from the initial crack present at the upper interface. However, some time later, shear cracks are also observed at the bottom interface. These cracks grow much faster and final failure is due to the fracture at the bottom interface. For layers of low modulus ($E_s = 10^6$ and $E_w = 10^5$ Pa) the initial crack velocities are approximately 40 m/s at the top interface. However, convergence difficulties prevented the solution from being completed. For E_s =

10^6 Pa and $E_w = 7 \times 10^5$ Pa the upper interface crack velocities are about 40-50 m/s. However, at the lower interface the velocities are much higher. In a slab of 15 cm thickness the crack growth is along the upper interface only and no cracks are seen at the bottom interface. The crack velocities along the top interface are similar to that for a thick slab. The crack propagation, for both thick and thin slabs, is mainly in mode II. The average upper interface velocities are inter-sonic but lower interface velocities are supersonic and need investigation.

REFERENCES

1. Albert, D.G., 1993. A comparison between wave propagation in water saturated and air saturated porous materials, J. Appl. Physics, 73 (1), pp. 28-36.
2. Bader, H.P., B. Salm., 1990. On the mechanics of snow slab release. Cold Regions Science and Technology, 17(3), 287-300.
3. Johnson, B.C., Jamieson, J.B., Stewart, R.R., 2004. Seismic measurements of fracture speed in a weak snowpack layer, Cold Regions Science and Technology, 40(1-2), 41-45.
4. Johnson, J.B., 1982. On the application of Biot's theory to acoustic wave propagation in snow, Cold Regions Science and Technology, Volume 6, Issue 1, P. 49 - 60.
5. Kirchner, H.O.K.,G.Michot., J. Schweizer, 2002. Fracture toughness of snow in shear and tension, Scripta Materialia, 46(6), 425-429.
6. Mahajan, P., Brown, R.L., 1993. A Microstructure Based Constitutive Law for Snow, Annals of Glaciology, p287-294.
7. Mahajan, P., Senthil, S., 2004. Cohesive element modeling of crack growth in a layered snowpack Cold Regions Science and Technology, Volume 40(1-2), 111-122.
8. McClung, D.M., 2005. Approximate estimates of fracture speeds for dry slab avalanches, Geophysical Research Letters, 32, Ll08406.
9. Mellor, M., 1975. A Review of Basic Snow Mechanics, Proc. of International Symposium on Snow Mechanics, Grindewald, IAHS Publ. 114, 251-259.
10. Needleman, A., Rosakis, A. J., 1999. The effect of bond strength and loading rate on the conditions governing the attainment of intersonic crack growth along interfaces, J. Mech. Phys. Solids, vol. 47, 2411-2449.
11. Rahulkumar,P.A., Jagota, S.J., Bennison, Saigal, S., 2000. Cohesive element modeling of viscoelastic fracture: application to peel testing of polymers. International Journal of Solids and Structures 3 (13), 1873– 1897.
12. Schweizer, J., 2004. Skier-triggered avalanches: observations and concepts. In: K. Kristensen (Editor), Proceedings Snoskred og friluftsliv, Stryn, Norway, 24-27 October 2002: pp. 52-55.
13. van Herwijnen, A. and Jamieson, B., 2005. High-speed photography of fractures in weak snowpack layers**,** Cold Regions Science and Technology, 43(1-2), 71-82.
14. Wilson, A., J. Schweizer, C. D. Johnston, J. B. Jamieson, 1999. Effects of surface warming of a dry snowpack, Cold Regions Science and Technology, 30, 59–65.
15. Xu, X.P., Needleman,A., 1994. Numerical Simulation of Fast Crack Growth in Brittle Solids, J. Mech. Phys. Solids, 42, 1397-1434.